



## Short communication

## Activity and molecular modeling of a new small molecule active against NNRTI-resistant HIV-1 mutants

Antonio Carta<sup>a,\*</sup>, Sabrina Pricl<sup>b</sup>, Sandra Piras<sup>a</sup>, Maurizio Fermeglia<sup>b</sup>, Paolo La Colla<sup>c</sup>, Roberta Loddo<sup>c</sup><sup>a</sup> Dipartimento Farmaco Chimico Tossicologico, Università di Sassari, Via Muroni 23/a, 07100 Sassari, Italy<sup>b</sup> Laboratorio MOSE, Dipartimento di Ingegneria Chimica, Piazzale Europa 1, 34127 Trieste, Italy<sup>c</sup> Dipartimento di Scienze e Tecnologie Biomediche, Sezione di Microbiologia e Virologia Generale e Biotecnologie Microbiche, Università di Cagliari, Cittadella Universitaria, 09042 Monserrato (Cagliari), Italy

## ARTICLE INFO

## Article history:

Received 26 June 2009

Received in revised form

18 August 2009

Accepted 20 August 2009

Available online 4 September 2009

## Keywords:

HIV

NNRTI resistant mutants

HIV-1wt RT assay

Molecular modeling

## ABSTRACT

In this preliminary study we report the antiviral screening of triazolo[4,5-g]quinoline derivatives (compounds **1–6**). 4,9-Dihydrotriazolo[4,5-g]quinoline-1-oxide (**1**) stood out as a new, small molecule endowed with a selective, promising activity in cell-based assays against HIV-1wt and clinically relevant NNRTI resistant mutants. In order to identify the molecular target, compound **1** was assayed in enzyme assay against the HIV-1wt RT. The molecular modeling strategy adopted yielded a rationale, in terms of molecular interactions and free energy of binding, for the possible reasons of the activity of this compound against NNRTI-resistant HIV-1 mutants with the RT isoforms K103N and Y181C.

© 2009 Elsevier Masson SAS. All rights reserved.

## 1. Introduction

A major challenge facing medicinal chemistry over the last few years has been (and still remains) the development of antiretroviral drugs endowed with significantly improved cross-resistance profiles, high barrier to resistance and/or new modes of action for chronic use in combination therapies.

Important components of the highly active antiretroviral therapy (HAART) are non-nucleoside inhibitors targeted at Human Immunodeficiency Virus (HIV) reverse transcriptase (NNRTIs). The very high affinity and selectivity of these molecules for the HIV-1 RT, over that for HIV-2 RT and cellular polymerases, contributes to their lower cytotoxicity levels. However, their very high affinity for the HIV-1 non-nucleoside binding site (NNBS) renders the different classes of NNRTIs capable to induce the rapid selection of NNRTI resistant variants.

All reported NNRTI-induced mutations occur in residues surrounding their binding pocket. Clinically significant NNRTI resistant variants are those carrying either or both the point

mutations Y181C and K103N, which are rapidly selected *in vivo* and confer broad spectrum resistance to most of the NNRTIs.

As part of our antiviral research program, we have recently synthesized and tested *in vitro* a series of new angular and linear *N*-tricyclic systems against representatives of both ssRNA<sup>+</sup> viruses [Bovine Viral Diarrhea Virus (BVDV), Yellow Fever Virus (YFV), Coxsackie B2 (CVB-2), Polio [Sb-1] and Human Immunodeficiency Virus (HIV-1)], ssRNA<sup>-</sup> viruses [Respiratory Syncytial Virus (RSV) and Vesicular Stomatitis Virus (VSV)], dsRNA viruses [Reovirus (Reo-1)], and DNA viruses [Vaccinia Virus (VV)] [1–4].

In this work, we present the results obtained in a study aimed at the design, synthesis and antiviral activity evaluation of triazolo[4,5-g]quinoline derivatives (compounds **1–6**, Fig. 1). One of them – 4,9-dihydro-triazolo[4,5-g]quinoline-1-oxide (**1**) – exhibited interesting activity against wild-type (wt) HIV-1, as well as against single, double and triple mutant variants of HIV-1. Using a computational procedure based on an ensemble of molecular modeling/simulation techniques, we docked **1** in the HIV-1 NNBS and calculated the relevant free energy of binding to the RT.

4,9-Dihydrotriazolo[4,5-g]quinoline-1-oxide (**1**), 1-ethoxy-4,9-dihydrotriazolo[4,5-g]quinoline (**2**), 4-chlorotriazolo[4,5-g]quinoline-1-oxide (**3**), 4,9-dihydrotriazolo[4,5-g]quinoline (**4**), triazolo[4,5-g]quinoline (**5**), and 5,6,7,8-tetrahydrotriazolo[4,5-g]quinoline (**6**) were prepared according to the procedure previously described [5–7].

**Abbreviations:** ssRNA<sup>+</sup>, single-stranded positive-sense RNA genome; dsRNA, double-stranded RNA genome; ssRNA<sup>-</sup>, negative-sense RNA genome; wt, wild-type; NNRTI, Non-Nucleoside Reverse Transcriptase Inhibitors; NNBS, Non-Nucleoside Binding Site.

\* Corresponding author. Tel./fax: +39 079 228720.

E-mail address: [acarta@uniss.it](mailto:acarta@uniss.it) (A. Carta).

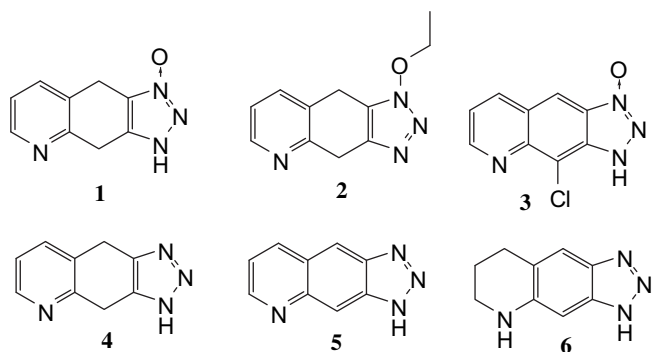


Fig. 1. Triazolo[4,5-g]quinoline derivatives (1–6).

## 2. Results and discussion

Compounds (1–6) were evaluated in cell-based assays against the above listed ssRNA<sup>+</sup>, dsRNA and ssRNA<sup>-</sup> viruses, as previously described [1–4]. Cytotoxicity of compounds was evaluated in parallel with the antiviral activity.

As shown in Table 1, none of the triazolo[4,5-g]quinoline inhibited RNA or DNA virus multiplication in cytopathogenicity or plaque reduction assays, with the sole exception of compound 1, which exhibited activity, in the micromolar range, against HIV-1wt. More interestingly, compound 1 was also the sole compound endowed with activity against HIV-1 variants carrying single, double and triple mutations (Table 2). In order to identify the molecular target, compound 1 was assayed in enzyme assays against the HIV-1wt RT [8]. Assays were undertaken with quality controls to ensure optimal performance. These include IC<sub>50</sub> determination for a known inhibitor (efavirenz) as a positive control. Compound 1 was confirmed to inhibit HIV-RT in a dose dependent manner (Fig. 2), it turned out to be active at  $19 \pm 3$  nM (efavirenz, used as reference drug, was active at  $1.3 \pm 0.3$  nM).

Compound 1 shows discrepant antiviral activity between enzymatic and cell-based assays. Several possibilities may be raised; (i) insufficiency of cellular uptake, (ii) degradation in our cell-based assay, (iii) protein binding(s), and (iv) others. Since chemical structure of compound 1 seems to be rigid and stable [5], it is unlikely that compound 1 has a property of easy and/or rapid degradation by factors including cellular enzymes. It is also possible that compound 1 has some protein binding activity as described [9]. Not only serum protein bindings, it might bind to HIV-1 envelope protein, gp120. To date, several compounds reported as RT [10] and integrase [11] inhibitors have been revealed as entry inhibitors. In

Table 1  
Antiviral activity (EC<sub>50</sub>)<sup>c</sup> of compounds 1–6 and reference compounds, against HIV-1<sub>IIIb</sub>, BVDV, YFV, CVB-2, Sb-1, Reo-1, VSV and VV.

|                    | 1          | 2    | 3    | 4    | 5    | 6    | NVP | EFV   |
|--------------------|------------|------|------|------|------|------|-----|-------|
| BVDV <sup>a</sup>  | >100       | >100 | >100 | >100 | >100 | >100 |     |       |
| YFV <sup>a</sup>   | >100       | >100 | >100 | >100 | >100 | >100 |     |       |
| CVB-2 <sup>b</sup> | >100       | >100 | >100 | >100 | >100 | >100 |     |       |
| Sb-1 <sup>b</sup>  | >100       | >100 | >100 | >100 | >100 | >100 |     |       |
| HIV-1 <sup>a</sup> | $12 \pm 1$ | >100 | >100 | >100 | >100 | >100 | 0.3 | 0.002 |
| RSV <sup>b</sup>   | >100       | >100 | >100 | >100 | >100 | >100 |     |       |
| VSV <sup>b</sup>   | >100       | >100 | >100 | >100 | >100 | >100 |     |       |
| Reo-1 <sup>a</sup> | >100       | >100 | >100 | >100 | >100 | >100 |     |       |
| VV <sup>b</sup>    | >100       | >100 | >100 | >100 | >100 | >100 |     |       |

<sup>a</sup> Compound concentration ( $\mu$ M) required to achieve 50% protection from virus-induced cytopathogenicity, as determined by the MTT method.

<sup>b</sup> Compound concentration ( $\mu$ M) required to reduce the virus plaque number by 50%.

<sup>c</sup> Data represent mean values ( $\pm$ SD) for three independent determinations.

Table 2

Cytotoxicity<sup>a</sup> (CC<sub>50</sub>)<sup>c</sup> against MT-4 cells and antiviral activity<sup>b</sup> (EC<sub>50</sub>) of compounds 1–6 and reference compounds, against HIV-1 variants containing the mutations Y181C (N119), K103N + Y181C (A17) and K103R + V179D + P225H (EFV<sup>R</sup>).

|                  | 1           | 2    | 3    | 4    | 5    | 6    | NVP  | EFV  |
|------------------|-------------|------|------|------|------|------|------|------|
| MT-4             | >100        | >100 | >100 | >100 | >100 | >100 | >100 | 45   |
| N119             | $4 \pm 0.2$ | >100 | >100 | >100 | >100 | >100 | 7    | 0.01 |
| A17              | $10 \pm 1$  | >100 | >100 | >100 | >100 | >100 | >20  | 0.06 |
| EFV <sup>R</sup> | $9 \pm 0.5$ | >100 | >100 | >100 | >100 | >100 | >20  | 7    |

<sup>a</sup> Compound concentration ( $\mu$ M) required to reduce the viability of mock-infected MT-4 cells by 50%, as determined by the MTT method.

<sup>b</sup> Compound concentration ( $\mu$ M) required to achieve 50% protection from virus-induced cytopathogenicity, as determined by the MTT method.

<sup>c</sup> Data represent mean values ( $\pm$ SD) for three independent determinations.

this study, structural data are well correlated with biochemical results, therefore, at least, compound 1 acts as an NNRTI *in vitro*. Further experiments are indeed needed to clarify the mechanism of action and generate more potent derivatives.

Compound 1 was then modeled and docked into the HIV-1 RT NNBS. Generally speaking, there are two key requirements for the computer-aided structure-based drug design methods:

- The generation of correct conformations of docked ligands, and
- The accurate prediction of binding affinity.

To check whether our procedure complied with requirement (i), we modeled and docked nevirapine, for which the crystallographic structure in complex with HIV-1 RT is available [12], as a reference system. This was basically done by removing the inhibitor from its binding site, building a new molecular model for this compound, applying the conformational procedure previously described [13], and finally docking it back into the protein NNBS. The best docked structure (i.e., the configuration with the lowest docking energy in a prevailing cluster), was then compared with the corresponding

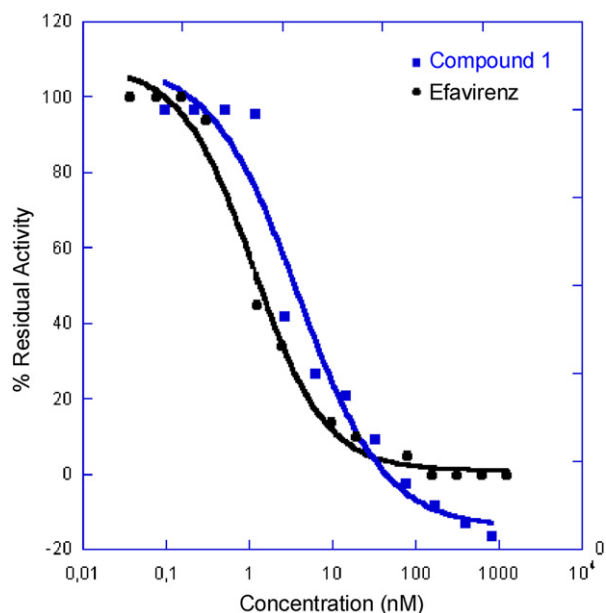
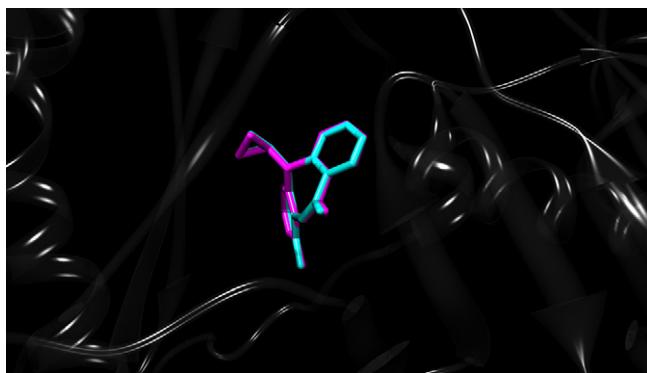


Fig. 2. Dose–response curve displaying the IC<sub>50</sub> (nM) of compound 1 in a RT assay. Data analysis and presentation: all data are presented as the averages of three independent experiments and standard deviations were less than 20%. % Residual activity was plotted versus increasing concentration of compounds. The curve was fit with Kaleidagraph (Synergy Software) to obtain IC<sub>50</sub> values.



**Fig. 3.** Detailed view of the comparison between the co-crystallized conformation of nevirapine into the HIV-RT NNBS (cyan sticks) and the corresponding docked conformation of nevirapine in the same enzyme pocket obtained upon application of the computational strategy adopted in this work (magenta sticks).

crystal structure. Fig. 3 shows a comparison between the co-crystallized conformation of nevirapine in the HIV-1 RT NNBS and the docked conformation obtained upon application of the computational strategy adopted in this work. At a first glance it can be seen that the agreement between the two structures is excellent: the root-mean-square deviation (RMSD) between the docked configuration and the relevant crystal structures of this test inhibitor is equal to 0.08 Å.

The calculated value of the free energy of binding for nevirapine after docking and the applications of the MM/PBSA procedure is  $\Delta G_{\text{bind}} = -9.74$  kcal/mol, which corresponds to an  $\text{IC}_{50}$  value of 0.073  $\mu\text{M}$ . The determined experimental  $\text{IC}_{50}$  value is 0.084–0.09  $\mu\text{M}$ , equivalent to  $\Delta G_{\text{bind}} = -9.62$  kcal/mol [14–16]. To double check the validity of the procedure, efavirenz was also subjected to the same computational protocol. The last two rows of Table 3 list the estimated  $\Delta G_{\text{bind}}$  and  $\text{IC}_{50}$  values for this HIV-RT inhibitor: considering the experimental value of  $\text{IC}_{50} = 0.0029$   $\mu\text{M}$  [18] and, hence, the corresponding value of  $\Delta G_{\text{bind}} = -11.64$  kcal/mol, we readily see that, once again, the agreement between *in vitro* and *in silico* data is very good. In the light of these positive blank-test results, our modeling/docking procedure was applied for predicting the binding mode of compound **1**. Fig. 4(A) and (B) show the equilibrated pose of **1** in the HIV-RT NNBS after the sequential application of our docking and MM/PBSA procedures.

Quantitative information about the forces involved in substrate binding can be obtained by analyzing the values of the free energy of binding  $\Delta G_{\text{bind}}$  and its components, which are listed in Table 3. As can be seen, both the intermolecular van der Waals interactions and the electrostatics are important contributions to the binding. However, the electrostatic desolvation penalty ( $\Delta G_{\text{PB}}$ ) offsets the favorable (i.e., negative) intermolecular electrostatics ( $\Delta E_{\text{EL}}$ ), yielding an unfavorable net electrostatic contribution to

the compound affinities for the enzyme. Accordingly, the association between **1** and HIV-1RT is mainly driven by the more favorable non-polar interactions present in the complex than in solution.

Interestingly, the N-oxide group is involved in two fluctuating alternate hydrogen bonds. The first H-bond involves the oxygen atom as an acceptor, and the hydrogen of the HN backbone group of F227 as the donor, and is characterized by an average dynamic length (ADL) of 2.64 Å. The second H-bond involves again the oxygen atom of the N-oxide group as an acceptor and the hydrogen atom of the NH backbone moiety of L234 as the donor, with an ADL = 2.89 Å (see Fig. 4(C)).

Further insights into the binding mode of **1** into the NNBS can be gained by considering the decomposition of the free energy of binding on a residue basis. To this purpose, Table 4 lists some of the residues that interact most favorably with the inhibitor. The values for residues K103 and Y181 are also listed for comparison.

The two residues involved in H-bonds with the inhibitor are also characterized by highly favorable values of the van der Waals terms. Further, the interaction of F227 with **1** is also stabilized by electrostatic forces, due to the presence of the aromatic ring in the side chain. The two residues most often found mutated NNRTI resistant mutants only poorly interact with the above inhibitor, both from the dispersion and the Coulombic forces standpoint. This might constitute a proof for the fact that compound **1** is not affected by the presence of the mutated residues in the protein.

Besides the several van der Waals and hydrophobic interactions that this molecule can form with the residues making up the enzyme binding site, Fig. 4 reveals the presence of important  $\pi$ – $\pi$  stabilizing interactions occurring between the condensed ring system of **1** and the aromatic rings of several residues lining the NNBS of the HIV-1 RT, resulting from the parallel-displaced geometry of these residues. The electronic nature of the  $\pi$ – $\pi$  interactions indeed favors the stacking of aromatic rings either by parallel-displaced (off-center) or edge-on (T-stacking) geometries, while the face-to-face geometry is unfavorable (particularly in environments where there is a low effective dielectric constant), since the dominant interaction is  $\pi$ -electron repulsion (Fig. 4(C)). This is well testified by the values reported in Table 4 for the residues mainly involved in these types of interactions with **1**.

As can be inferred from the values shown in Table 4, compound **1** has the strongest contacts with residues not commonly associated with NNRTI resistance. Indeed, when considering the sum of both energy components for each residue reported in Table 4, i.e.,  $\Delta E_{\text{MM(Res.)}} = \Delta E_{\text{VDW(Res.)}} + \Delta E_{\text{EL(Res.)}}$ , it can be realized that there are 4 residues which present an extremely favorable interactions (20–30 kcal/mol) with **1**: Y188 ( $\Delta E_{\text{MM(Res.)}} = -27.79$  kcal/mol), F227 (–25.30 kcal/mol), H96 (–20.79 kcal/mol), and Y183 (–19.75), and none of these amino acids is among the clinically relevant ones involved in HIV drug resistance. On the contrary, for residue Y181,

**Table 3**

Free energy components and total binding free energies for **1**, nevirapine and efavirenz and HIV-1 RT. All energies are in kcal/mol.  $\text{IC}_{50}$  values in  $\mu\text{M}$ .

|              | $\Delta E_{\text{VDW}}$ | $\Delta E_{\text{EL}}$ | $\Delta G_{\text{PB}}$ | $\Delta G_{\text{NP}}$ | $-T\Delta S$ | $\Delta G_{\text{bind}}$ | $\text{IC}_{50}^a$ |
|--------------|-------------------------|------------------------|------------------------|------------------------|--------------|--------------------------|--------------------|
| <b>1</b>     |                         |                        |                        |                        |              |                          |                    |
| –33.23 ± 0.4 | –24.47 ± 0.2            | 39.45 ± 0.7            | –5.13 ± 0.0            | 16.29 ± 0.5            | –7.09 ± 0.4  | 6.3                      |                    |
| nevirapine   |                         |                        |                        |                        |              |                          |                    |
| –39.01 ± 0.3 | –33.20 ± 0.2            | 54.94 ± 0.5            | –5.10 ± 0.1            | 12.63 ± 0.4            | –9.74 ± 0.3  | 0.073                    |                    |
| efavirenz    |                         |                        |                        |                        |              |                          |                    |
| –42.73 ± 0.4 | –30.20 ± 0.3            | 52.21 ± 0.5            | –4.52 ± 0.0            | 13.33 ± 0.5            | –11.91 ± 0.5 | 0.0018                   |                    |

<sup>a</sup> Calculated  $\text{IC}_{50}$  values are obtained from the corresponding  $\Delta G_{\text{bind}}$  values using the following relationship:  $\Delta G_{\text{bind}} \cong RT \ln \text{IC}_{50}$  [17], where  $R$  is the ideal gas constant and  $T$  is temperature in K.

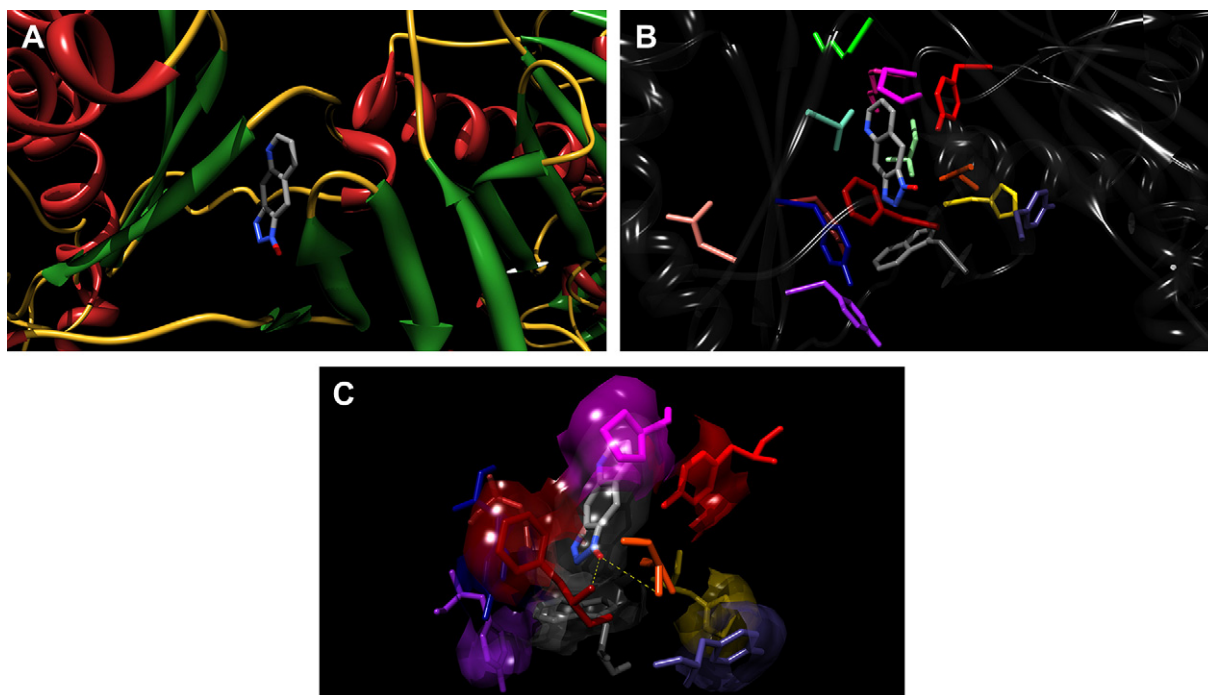


**Fig. 4.** (A) View of compound **1** docked in the NNBS of HIV-RT. The docked model was obtained using the combined AutoDock/MM/PBSA strategy adopted in this work. The inhibitor is in atom-colored stick representation (carbon, gray; nitrogen, blue, oxygen, red). The secondary structure of the protein is depicted as a colored ribbon (helices, firebrick; strands, forest green; coils, golden rod). Hydrogen atoms, counterions, and water molecules are omitted for clarity. (B) Details of the binding mode of compound **1** in HIV-RT NNBS. The color coding for the protein residues is the following: H96, gold; L100, light green; K101, dark pink; K103, green; V106, aquamarine; L109, salmon; Y181, brown; Y183, purple; Y188, navy blue; F227, dark red; W229, dim gray; Y232, dark slate blue; L234, orange red; P236, magenta; Y318, red. (C) Graphical portrait of the two, alternate hydrogen bonds between **1** and F227 and L234, respectively (yellow broken lines), and of the stabilizing  $\pi$ - $\pi$  interactions between **1** and all aromatic residues lining the binding site (depicted as interaction surfaces). Color code as in (B).

**Table 4**

Individual contributions of selected residues to binding of **1** to HIV-1 RT. Clinically relevant mutant residues are highlighted in bold. All energies are in kcal/mol.

| Res. | $\Delta E_{VDW}$ | $\Delta E_{EL}$ | Res. | $\Delta E_{VDW}$ | $\Delta E_{EL}$ |
|------|------------------|-----------------|------|------------------|-----------------|
| H96  | -10.8            | -10.0           | Y188 | -14.7            | -13.1           |
| K103 | <b>-3.6</b>      | <b>-11.2</b>    | F227 | -13.4            | -11.9           |
| L109 | -7.3             | -3.3            | Y232 | -7.5             | -11.3           |
| Y181 | <b>-1.6</b>      | <b>-0.8</b>     | L234 | -10.0            | -2.7            |
| Y183 | -7.8             | -12.0           | P236 | -8.6             | -6.2            |

$\Delta E_{MM(Res.)}$  is only equal to  $-2.36$  kcal/mol, whilst for the other, important NNRTI resistant site, K103,  $\Delta E_{MM(Res.)} = -14.73$  kcal/mol. These observations clearly support the remarkable activity of compound **1** towards NNRTI HIV-RT mutants, as highlighted in Table 2.

### 3. Conclusions

In summary, we discovered that 4,9-dihydrotriazolo[4,5-g]quinoline-1-oxide (**1**) is a new small molecule targeting the HIV-1 RT, endowed with selective activity against wild-type and clinically relevant NNRTI resistant mutants. Derivative **1** showed no cytotoxicity and very selective activity against HIV-1, whereas it resulted completely inactive against all the other RNA viruses tested. SAR evidences suggest that the triazolo[4,5-g]quinoline scaffold owes its antiretroviral activity to the oxygen atom linked at *N*-1 of the triazolo moiety as well as to the non-planar central ring,  $sp^3$  hybridization of the C-4 and C-9, in fact on the contrary compound **3** is completely inactive. Finally, the molecular modeling strategy adopted yielded a rationale, in terms of molecular interactions and free energy of binding, for the possible reasons of the insensitivity of this compound towards the mutated HIV-1 RT isoforms (K103N and Y181C).

Further SAR investigations and biological experiments will be reported in due course.

## 4. Experimental protocols

### 4.1. Melting points, analytical and spectroscopical data

Intermediates and final compounds **1–6** were prepared according to the procedure previously described [5–7].

M.p.s were uncorrected and were taken in open capillaries in a Digital Electrothermal IA9100 melting point apparatus. LC/MS spectra were performed on a combined Liquid Chromatograph-Agilent 1100 series Mass Selective Detector (MSD). Analyses indicated by the symbols of the elements were within  $\pm 0.4\%$  of the theoretical values.

| Compd    | Anal.              | M.p.              | LC/MS   |
|----------|--------------------|-------------------|---------|
| <b>1</b> | $C_9H_8N_4O$       | $>300^\circ C$    | 189     |
|          | C,H,N              | (ethanol)         | (M + H) |
| <b>2</b> | $C_{11}H_{12}N_4O$ | 144–145 °C        | 217     |
|          | C,H,N              | (acetone)         | (M + H) |
| <b>3</b> | $C_9H_5ClN_4O$     | $>300^\circ C$    | 221     |
|          | C,H,N,Cl           | (ethanol)         | (M + H) |
| <b>4</b> | $C_9H_8N_4$        | 226–228 °C (dec.) | 173     |
|          | C,H,N              | (acetone)         | (M + H) |
| <b>5</b> | $C_9H_6N_4$        | 211–212 °C        | 171     |
|          | C,H,N              | (acetone)         | (M + H) |
| <b>6</b> | $C_9H_6N_4$        | 164–166 °C        | 175     |
|          | C,H,N              | (ethanol)         | (M + H) |

$^1\text{H}$  NMR spectra were recorded on a Varian XL-200 (200 MHz) instrument, using TMS as internal standard. The chemical shift values are reported in ppm ( $\delta$ ) and coupling constants ( $J$ ) in Hertz (Hz). Signal multiplicities are represented by: s (singlet), d (doublet), dd (double doublet), t (triplet), q (quadruplet), m (multiplet).

| Compd | $^1\text{H}$ NMR (solvent):  |
|-------|--|
| 1     | (DMSO- $d_6$ ): $\delta$ 8.41 (d, 1H, $J$ = 4.8 Hz, H-6), 7.68 (d, 1H, $J$ = 7.0 Hz, H-8), 7.23 (dd, 1H, $J$ = 7.0 and 4.8 Hz, H-7), 3.94 (m, 2H, C <sub>4</sub> -H <sub>2</sub> ), 3.76 (m, 2H, C <sub>9</sub> -H <sub>2</sub> ).   |
| 2     | (CDCl <sub>3</sub> ): $\delta$ 8.57 (d, 1H, $J$ = 4.6 Hz, H-6), 7.64 (d, 1H, $J$ = 8.0 Hz, H-8), 7.23 (dd, 1H, $J$ = 8.0 and 4.6 Hz, H-7), 4.59 (q, 2H, $J$ = 7.0 Hz, O-CH <sub>2</sub> ), 4.31 (m, 2H, C <sub>4</sub> -H <sub>2</sub> ), 4.09 (m, 2H, C <sub>9</sub> -H <sub>2</sub> ), 1.47 (t, 3H, $J$ = 7.0 Hz, CH <sub>3</sub> ). |
| 3     | (DMSO- $d_6$ ): $\delta$ 9.10 (d, 1H, $J$ = 4.2 Hz, H-6), 8.68 (d, 1H, $J$ = 8.8 Hz, H-8), 8.46 (s, 1H, H-9), 7.65 (dd, 1H, $J$ = 8.8 and 4.2 Hz, H-7).  |
| 4     | (DMSO- $d_6$ ): $\delta$ 8.82 (d, 1H, $J$ = 5.2 Hz, H-6), 8.50 (d, 1H, $J$ = 7.6 Hz, H-8), 7.92 (dd, 1H, $J$ = 7.6 and 5.2 Hz, H-7), 4.50 (m, 2H, C <sub>4</sub> -H <sub>2</sub> ), 4.32 (m, 2H, C <sub>9</sub> -H <sub>2</sub> ).   |
| 5     | (DMSO- $d_6$ ): $\delta$ 9.42 (d, 1H, $J$ = 4.4 Hz, H-6), 9.31 (d, 1H, $J$ = 8.0 Hz, H-8), 9.12 (s, 1H, H-4), 8.77 (s, 1H, H-9), 7.99 (dd, 1H, $J$ = 8.0 and 4.4 Hz, H-7).   |
| 6     | (DMSO- $d_6$ ): $\delta$ 14.65 (s, 1H, NH), 7.43 (s, 1H, H-9), 6.52 (s, 1H, H-4), 3.24 (t, 2H, $J$ = 5.6 Hz, C <sub>6</sub> -H <sub>2</sub> ), 2.83 (t, 2H, $J$ = 5.6 Hz, C <sub>8</sub> -H <sub>2</sub> ), 1.80 (m, 2H, C <sub>7</sub> -H <sub>2</sub> ).   |

#### 4.2. Antiviral assays

Activity of compounds against Human Immunodeficiency Virus type-1 (HIV-1) was based on inhibition of virus-induced cytopathogenicity in MT-4 cells acutely infected with a multiplicity of infection (m.o.i.) of 0.01. Briefly, 50  $\mu\text{L}$  of RPMI containing  $1 \times 10^4$  MT-4 were added to each well of flat-bottom microtitre trays containing 50  $\mu\text{L}$  of RPMI, without or with serial dilutions of test compounds. Then, 20  $\mu\text{L}$  of an HIV-1 suspension containing 100 CCID<sub>50</sub> were added. After a 4-day incubation, cell viability was determined by the MTT method [19]. Compound cytotoxicity was evaluated in parallel with antiviral activity, based on the viability of mock-infected cells as monitored by the MTT method.

#### 4.3. Enzyme assays

RT assays were performed using a non radioactive method as previously described [8]. Purified HIV-RT was purchased from Ambion and assayed for its RNA-dependent polymerase-associated activity in a 20  $\mu\text{L}$  volume containing: 60 mM Tris-HCl (pH 8.1), 60 mM KCl, 8 mM MgCl<sub>2</sub>, 13 mM DTT, 2.5 ng  $\mu\text{L}^{-1}$  template: primer [poly(A)-oligo(dT)<sub>16</sub>] and 100  $\mu\text{M}$  dTTP. After incubation for 30 min at 37 °C, reactions were stopped by addition of 2  $\mu\text{L}$  of 200 mM EDTA. 138  $\mu\text{L}$  of PicoGreen Quantitation Reagent (Molecular Probes), diluted 1/345 in TE, was added to each sample and incubated at room temperature, protected from ambient light, for 5 min. Fluorescence of samples in wells of a 96-well microtiter plate was determined in a fluorescence microplate reader (VICTOR<sup>3</sup> Multilabel Plate Reader, PerkinElmer).

#### 4.4. Molecular modeling

The original 3D structure of the RT in complex with nevirapine (PDB code 1FKP) [12], including the 178 crystallographic water molecules, was used as a starting point. Wild-type residue K103 was introduced into the 103N crystal structure of RT/nevirapine complex using the Biopolymer module of Insight II by swapping the mutant residue into the specific site following our validated

procedure [20]. The complex was then minimized using the *Sander* module of AMBER 9 [21], and the *parm94* all-atom force field of Cornell et al. [22]. Eventual missing force field parameters for **1** were generated by QM calculations.

To set up the complex for the simulation, we adopted the following ansatz: first, to let the protein relax in an aqueous environment, the complex was immersed in a 75-Å radius sphere of TIP3P water molecules [23]. The resulting system was minimized with a gradual decrease in the position restraints of the protein atoms. At the end of the relaxation process, all water molecules beyond the first hydration shell (i.e., at a distance >3.5 Å from any protein atom) were removed. Finally, to achieve electroneutrality, a suitable number of counterions were added, in the positions of largest electrostatic potential, as determined by command *addlons* of the *LEaP* module within AMBER 9. To reduce computational time to reasonable limits, all proteins residues with any atom closer than 30 Å from the center of mass of the inhibitor were chosen to be flexible in the dynamic simulations. Subsequently, a spherical TIP3P water cap of radius equal to 30 Å was centered on **1** in the corresponding complex, including the hydrating water molecules within the sphere resulting from the previous step. After energy minimization of the new water cap for 1500 steps, keeping the protein, the inhibitor, and the pre-existing waters rigid, followed by a molecular dynamics (MD) equilibration of the entire water sphere with fixed solute for 20 ps, further unfavorable interactions within the structures were relieved by progressively smaller positional restraints on the solute (from 25 to 0 kcal/mol Å<sup>2</sup>) for a total of 4000 steps.

The system was gradually heated to 300 K in three intervals, allowing a 5 ps interval per each 100 K, and then equilibrated for 50 ps at 300 K, followed by 400 ps of data collection runs, necessary for the estimation of the free energy of binding (*vide infra*). After the first 20 ps of MD equilibration, additional TIP3P water molecules were added to the 30 Å water cap to compensate for those who were able to diffuse into gaps of the enzyme. The MD simulations were performed at constant  $T = 300$  K using the Berendsen coupling algorithm with separate coupling of the solute and solvent to the heat [24], an integration time step of 2 fs, and the applications of the SHAKE algorithm to constrain all bonds to their equilibrium values [25], thus removing high frequency vibrations. All intra-solute pairwise interactions, i.e., the bond, angle, dihedral, van der Waals and electrostatics terms of the molecular mechanics force field were accumulated without a distance-based cut-off. Long-range nonbonded interactions were truncated by using a dual cutoff of 12 and 30 Å, respectively, where energies and forces due to interactions between 12 and 30 Å were updated every 20 time step. The same frequency of update was employed for the nonbonded list. For the calculation of the binding free energy between HIV-1 RT and **1** in water, a total of 400 snapshots were saved during the MD data collection period described above, one snapshot per each 1 ps of MD simulation.

All energetic analysis was done for only a single MD trajectory of the RT/**1** complex, with unbound protein and substrate snapshots taken from the snapshots of that trajectory. According to the so-called molecular mechanics/Poisson-Boltzmann surface area method (MM/PBSA) [26], the binding free energy between **1** and HIV-1 RT can be calculated by Equation:  $\delta G_{\text{bind}} = \Delta E_{\text{MM}} + \Delta G_{\text{solv}} - T\Delta S$ .  $\Delta E_{\text{MM}}$  denotes the sum of molecular mechanics (MM) energies of the molecules, and can be further split into contributions from electrostatic ( $\Delta E_{\text{EL}}$ ) and van der Waals ( $\Delta E_{\text{vdW}}$ ) energies (i.e.,  $\Delta E_{\text{MM}} = \Delta E_{\text{EL}} + \Delta E_{\text{vdW}}$ ). The polar component of  $\Delta G_{\text{solv}}$  (i.e.,  $\Delta G_{\text{solv}} = \Delta G_{\text{PB}} + \Delta G_{\text{NP}}$ ) was evaluated with the Poisson-Boltzmann (PB) approach [13]. This procedure involves using a continuum solvent model, which represents the solute as a low dielectric medium (i.e., of dielectric constant  $\epsilon = 1$ ) with embedded charges and the solvent as a high dielectric medium ( $\epsilon = 80$ ) with no salt. All atomic charges were taken from the Cornell

et al. force field and from our *ab initio* calculations (see above), since these are consistent with the MM energy calculations. The dielectric boundary is the contact surface between the radii of the solute and the radius (1.4 Å) of a water molecule. The numerical solution of the linearized Poisson–Boltzmann equations was solved on a cubic lattice by using the iterative finite-difference method implemented in the DelPhi software package [27]. The grid size used was 0.5 Å. Potentials at the boundaries of the finite-difference lattice were set to the sum of the Debye–Hückel potentials. The non-polar contribution to the solvation energy was calculated as  $\Delta G_{\text{NP}} = \gamma (\text{SASA}) + \beta$ , in which  $\gamma = 0.00542 \text{ kcal}/\text{Å}^2$ ,  $\beta = 0.92 \text{ kcal/mol}$ , and SASA is the solvent-accessible surface estimated with the MSMS program [28].

The normal-mode analysis approach was followed to estimate the last parameter, i.e., the change in solute entropy upon association  $-T\Delta S$ . In the first step of this calculation, an 8-Å sphere around **1** was cut out from an MD snapshot for each inhibitor–protein complex. This value was shown to be large enough to yield converged mean changes in solute entropy. On the basis of the size-reduced snapshots of the complex, we generated structures of the uncomplexed reactants by removing the atoms of the protein and ligand, respectively. Each of those structures was minimized, using a distance-dependent dielectric constant  $\epsilon = 4r$ , to account for solvent screening, and its entropy was calculated using classical statistical formulas and normal-mode analysis. To minimize the effects due to different conformations adopted by individual snapshots we averaged the estimation of entropy over 10 snapshots.

## Acknowledgements

We acknowledge Dr Margherita Pezzullo for her collaboration in enzyme assays.

## References

- [1] A. Carta, G. Loriga, S. Piras, G. Paglietti, M. Ferrone, M. Fermeglia, S. Pricl, P. La Colla, B. Secci, G. Collu, R. Loddo, *Med. Chem.* 2 (2006) 577–589.
- [2] A. Carta, P. La Colla, R. Loddo, G. Paglietti, US patent, 60/871,352; 2006.
- [3] A. Carta, M. Loriga, G. Paglietti, M. Ferrone, M. Fermeglia, S. Pricl, T. Sanna, C. Ibba, P. La Colla, R. Loddo, *Bioorg. Med. Chem.* 15 (2007) 1914–1927.
- [4] A. Carta, M. Loriga, S. Piras, G. Paglietti, M. Ferrone, M. Fermeglia, S. Pricl, P. La Colla, G. Collu, T. Sanna, R. Loddo, *Med. Chem.* 3 (2007) 520–532.
- [5] A. Carta, G. Paglietti, *Arkivoc V* (2004) 66–75.
- [6] P. Sanna, A. Carta, G. Paglietti, *Heterocycles* 53 (2000) 423–432.
- [7] A. Carta, G. Paglietti, in: T.S. Kaufman, E.L. Larghi (Eds.), *Modern Approaches to the Synthesis of O- and N-Heterocycles*, vol. 1, Research Signpost: Keral, 2007, pp. 173–185.
- [8] A. Angusti, S. Manfredini, E. Durini, N. Ciliberti, S. Vertuani, N. Solaroli, S. Pricl, M. Ferrone, M. Fermeglia, R. Loddo, B. Secci, A. Visioli, T. Sanna, G. Collu, M. Pezzullo, P. La Colla, *Chem. Pharm. Bull. (Tokyo)* 56 (2008) 423–432.
- [9] M. Baba, S. Yuasa, T. Niwa, M. Yamamoto, S. Yabuuchi, H. Takashima, M. Ubasawa, H. Tanaka, T. Miyasaka, R.T. Walker, *Biochem. Pharmacol.* 45 (1993) 2507–2512.
- [10] R.W. Buckheit Jr., C. Lackman-Smith, M.J. Snow, S.M. Halliday, E.L. White, L.J. Ross, V.K. Agrawal, A.D. Broom, *Antivir. Chem. Chemother* 10 (1999) 23–32.
- [11] W. Plummers, N. Neamati, C. Pannecouque, V. Fikkert, C. Marchand, T.R. Burke Jr., Y. Pommier, D. Schols, E. De Clercq, Z. Debysier, M. Witvrouw, *Pharmacology* 58 (2000) 641–648.
- [12] J. Ren, J. Milton, K. Weaver, L.S.A. Short, D.I. Stuart, D.K. Stammers, *Structure Fold. Des.* 8 (2000) 1089–1094.
- [13] M.K. Gilson, K. Sharp, B.J. Honig, *Comput. Chem.* 9 (1987) 327–335.
- [14] V.J. Merluzzi, K.D. Hargrave, M. Labadia, K. Grozinger, M. Skoog, J.C. Wu, C.K. Shih, K. Eckner, S. Hattox, J. Adams, et al., *Science* 250 (1990) 1411–1413.
- [15] R.A. Koup, V.J. Merluzzi, K.D. Hargrave, J. Adams, K. Grozinger, R.J. Eckner, J.L. Sullivan, *Infect. Dis.* 163 (1991) 966–970.
- [16] E. De Clercq, *Antivir. Res.* 38 (1998) 153–179.
- [17] J. Wang, P. Morin, W. Wang, P.A. Kollman, *J. Am. Chem. Soc.* 123 (2001) 5221–5230.
- [18] S.D. Young, S.F. Britcher, L.O. Tran, L.S. Payne, W.C. Lumma, T.A. Lyle, J.R. Huff, P.S. Anderson, D.B. Olsen, S.S. Carroll, D.J. Pettibone, J.A. O'Brien, R.G. Ball, S.K. Balani, J.H. Lin, W. I-Chen, W.A. Schleif, V.V. Sardana, W.J. Long, V.W. Byrnes, E.A. Emini, *Antimicrob. Agents Chemother.* 39 (1995) 2602–2605.
- [19] R. Pauwels, et al., *J. Virol. Methods* 20 (1988) 309–317.
- [20] S. Pricl, M. Fermeglia, M. Ferrone, E. Tamborini, *Mol. Cancer Ther.* 4 (2005) 1167–1174.
- [21] D.A. Case, T.A. Darden, T.E. Cheatham III, C.L. Simmerling, J. Wang, R.E. Duke, R. Luo, K.M. Merz, D.A. Pearlman, M. Crowley, R.C. Walker, W. Zhang, B. Wang, S. Hayik, A. Roitberg, G. Seabra, K.F. Wong, F. Paesani, X. Wu, S. Brozell, V. Tsui, H. Gohlke, L. Yang, C. Tan, J. Mongan, V. Hornak, G. Cui, P. Beroza, D.H. Mathews, C. Schafmeister, W.S. Ross, P.A. Kollman, *AMBER 9*. University of California, San Francisco, CA, USA, 2006.
- [22] W.D. Cornell, P. Cieplak, C.I. Bayly, I.R. Gould, K.M. Merz, D.M. Ferguson, D.C. Spellmeyer, T. Fox, J.W. Caldwell, P.A. Kollman, *J. Am. Chem. Soc.* 117 (1995) 5179–5197.
- [23] W.L. Jorgensen, J. Chandrasekhar, J.D. Madura, R.W. Impey, M.L. Klein, *J. Chem. Phys.* 79 (1983) 926–935.
- [24] H.J.C. Berendsen, J.P.M. Postma, W.F. van Gunsteren, A. DiNola, J.R. Haak, *J. Chem. Phys.* 81 (1984) 3684–3690.
- [25] J.P. Ryckaert, G. Cicotti, H.J.C. Berendsen, *J. Comp. Phys.* 23 (1977) 327–341.
- [26] J. Srinivasan, T.E. Cheatham, P. Cieplak, P.A. Kollman, *J. Am. Chem. Soc.* 120 (1998) 9401–9409.
- [27] D. Sitkoff, K.A. Sharp, B.H. Honig, *J. Phys. Chem.* 98 (1994) 1978–1988.
- [28] M.F. Sanner, A.J. Olson, J.C. Spehner, *Biopolymers* 38 (1996) 305–320.